Environmental Science: Atmospheres

ROYAL SOCIETY OF CHEMISTRY

PAPER

View Article Online
View Journal | View Issue

Cite this: *Environ. Sci.: Atmos.*, 2024, **4**, 531

Temperature, humidity, and ionisation effect of iodine oxoacid nucleation

Birte Rörup,[a] Xu-Cheng He,*[ab] Jiali Shen,[ac] Rima Baalbaki,[a] Lubna Dada,[ad] Mikko Sipilä,[a] Jasper Kirkby,[ef] Markku Kulmala,[ag] Antonio Amorim,[h] Andrea Baccarini,[i] David M. Bell,[d] Lucía Caudillo-Plath,[f] Jonathan Duplissy,[ac] Henning Finkenzeller,[aw] Andreas Kürten,[f] Houssni Lamkaddam,[d] Chuan Ping Lee,[d] Vladimir Makhmutov,[jk] Hanna E. Manninen,[e] Guillaume Marie,[f] Ruby Marten,[d] Bernhard Mentler,[ab] Antti Onnela,[e] Maxim Philippov,[j] Carolin Wiebke Scholz,[l] Mario Simon,[f] Dominik Stolzenburg,[amn] Yee Jun Tham,[ao] António Tomé,[p] Andrea C. Wagner,[fq] Mingyi Wang,[r] Dongyu Wang,[d] Yonghong Wang,[as] Stefan K. Weber,[ef] Marcel Zauner-Wieczorek,[f] Urs Baltensperger,[d] Joachim Curtius,[f] Neil M. Donahue,[t] Imad El Haddad,[d] Richard C. Flagan,[u] Armin Hansel,[l] Ottmar Möhler,[v] Tuukka Petäjä,[a] Rainer Volkamer,[w] Douglas Worsnop[a] and Katrianne Lehtipalo[ax]

Iodine oxoacids are recognised for their significant contribution to the formation of new particles in marine and polar atmospheres. Nevertheless, to incorporate the iodine oxoacid nucleation mechanism into global simulations, it is essential to comprehend how this mechanism varies under various atmospheric conditions. In this study, we combined measurements from the CLOUD (Cosmic Leaving OUtdoor Droplets) chamber at CERN and simulations with a kinetic model to investigate the impact of temperature, ionisation, and humidity on iodine oxoacid nucleation. Our findings reveal that ion-induced particle formation rates remain largely unaffected by changes in temperature. However, neutral particle formation rates experience a significant increase when the temperature drops from +10 °C to −10 °C. Running the kinetic model with varying ionisation rates demonstrates that the particle formation rate only increases with a higher ionisation rate when the iodic acid concentration exceeds 1.5 × 10^7 cm^{-3}, a concentration rarely reached in pristine marine atmospheres. Consequently, our simulations suggest that, despite higher ionisation rates, the charged cluster nucleation pathway of iodic acid is unlikely to be enhanced in the upper troposphere by higher ionisation rates. Instead, the neutral nucleation channel is likely to be the dominant channel in that region. Notably, the iodine oxoacid nucleation mechanism remains unaffected by changes in relative humidity from 2% to 80%. However, under unrealistically dry conditions (below 0.008% RH at +10 °C), iodine oxides (I_2O_4 and I_2O_5) significantly enhance formation rates. Therefore, we conclude that iodine oxoacid nucleation is the dominant nucleation mechanism for iodine nucleation in the marine and polar boundary layer atmosphere.

Received 25th January 2024
Accepted 21st March 2024

DOI: 10.1039/d4ea00013g

rsc.li/esatmospheres

[a]*Institute for Atmospheric and Earth System Research/Physics, Faculty of Science, University of Helsinki, Helsinki, Finland. E-mail: xh346@cam.ac.uk*
[b]*Yusuf Hamied Department of Chemistry, University of Cambridge, Cambridge, UK*
[c]*Helsinki Institute of Physics, University of Helsinki, Helsinki, Finland*
[d]*Laboratory of Atmospheric Chemistry, Paul Scherrer Institute, Villigen, Switzerland*
[e]*CERN, European Organisation for Nuclear Research, Geneva, Switzerland*
[f]*Institute for Atmospheric and Environmental Sciences, Goethe University Frankfurt am Main, Frankfurt am Main, Germany*
[g]*Joint International Research Laboratory of Atmospheric and Earth System Sciences, School of Atmospheric Sciences, Nanjing University, Nanjing, China*
[h]*CENTRA, FCUL, University of Lisbon, Lisbon, Portugal*
[i]*Laboratory of Atmospheric Processes and their Impacts, École polytechnique fédérale de Lausanne, Lausanne, Switzerland*
[j]*Lebedev Physical Institute, Russian Academy of Sciences, Moscow, Russia*
[k]*Moscow Institute of Physics and Technology, National Research University, Moscow, Russia*
[l]*Institute for Ion and Applied Physics, University of Innsbruck, Innsbruck, Austria*
[m]*Institute for Materials Chemistry, TU Wien, Vienna, Austria*
[n]*Faculty of Physics, University of Vienna, Vienna, Austria*
[o]*School of Marine Sciences, Sun Yat-sen University, Zhuhai, China*
[p]*IDL-UBI, Universidade da Beira Interior, Covilhã, Portugal*
[q]*Aerosol Physics, Tampere University, Tampere, Finland*
[r]*Department of the Geophysical Sciences, University of Chicago, Chicago, USA*
[s]*State Key Joint Laboratory of Environment Simulation and Pollution Control, Research Center for Eco-Environmental Sciences, Chinese Academy of Sciences, Beijing, China*
[t]*Center for Atmospheric Particle Studies, Carnegie Mellon University, Pittsburgh, USA*
[u]*Division of Chemistry and Chemical Engineering, California Institute of Technology, Pasadena, USA*
[v]*Institute of Meteorology and Climate Research, Karlsruhe Institute of Technology, Karlsruhe, Germany*
[w]*Department of Chemistry & CIRES, University of Colorado Boulder, Boulder, USA*
[x]*Finnish Meteorological Institute, Helsinki, Finland*

Environmental significance

Understanding atmospheric new particle formation is of paramount importance, since it is impacting the climate. Particle formation through iodine oxoacid nucleation has rarely been incorporated into global simulations, despite observations at various coastal locations and increasing concentration of iodine, primarily driven by climate change. This study employs chamber measurements and a kinetic model to explore the influence of temperature, ionisation rate, and humidity on iodine oxoacid nucleation. Our findings indicate that ion-induced formation rates of iodine oxoacid are not significantly affected by temperature but the neutral formation rates increase with decreasing temperature. Furthermore, increases in ionisation rates decrease the ion-induced nucleation rate under atmospherically relevant iodic acid concentrations, and humidity has no significant effect on nucleation.

1 Introduction

Atmospheric aerosols are liquid or solid particles suspended in the air, which affect the global radiative budget directly by scattering and absorbing shortwave and longwave radiation, resulting in a direct radiative forcing.[1] Additionally, aerosols of sufficient size indirectly affect the climate by acting as cloud condensation nuclei (CCN). A change in CCN number may cause a change in the microphysical properties of clouds and thereby affecting the cloud lifetime, albedo and precipitation. A better understanding of the formation and growth of aerosol particles is especially needed since more than half of the global CCN originate from new particle formation processes in the atmosphere.[2]

New particle formation has been observed all over the world[3] at locations ranging from cities[4–7] to pristine regions like the Arctic,[8] Antarctica,[9] remote marine atmosphere,[10] and the boreal forest.[11,12] Sulphuric acid and organic vapours are believed to be the major contributors to new particle formation in the continental boundary layer and have been extensively researched.[13–15]

Iodine species have recently been proposed to be important for particle formation processes as well.[16–21] This has been observed in coastal[17–20,22] and polar environments.[23–25] Iodine precursors, emitted from the sea surface,[26] sea ice,[27] and macroalgae[18] are rapidly photolysed in the atmosphere to produce a series of iodine oxides (*e.g.*, iodine monoxide, IO and iodine dioxide, OIO) and oxoacids (*e.g.*, iodic acid, HIO_3 and iodous acid, HIO_2). The exact iodine particle formation mechanisms have been under debate for more than 20 years, with iodine oxides such as OIO, iodine tetroxide (I_2O_4) and iodine pentoxide (I_2O_5) initially thought to be the nucleating molecules.[17,18,28–31]

However, recent field observations at the Mace Head observatory have revealed the important role of HIO_3 in iodine particle formation processes.[19] Further experiments carried out at the Cosmics Leaving OUtdoor Droplets (CLOUD) chamber at CERN found that HIO_3 is produced from oxidised iodine in the presence of ozone and water vapour,[16] and iodooxy hypoiodite (I_2O_2) is the critical precursor for producing HIO_3.[32] This simple and efficient production pathway of HIO_3 may help explain the ubiquitous presence of HIO_3 globally,[16] even including inland polluted cities such as Beijing and Nanjing.[33]

The CLOUD experiment has also revealed that HIO_3 alone is not able to explain iodine particle formation and HIO_2 is needed to form the initial clusters together with HIO_3 (termed the iodine oxoacid nucleation mechanism).[16] Recent theoretical work utilising quantum chemical calculations and kinetic simulations further uncovered the critical role of HIO_2 in stabilising HIO_3 clusters because HIO_2 exhibits strong alkaline-like behaviour.[34,35] The fact that iodine oxidation produces both HIO_3 and HIO_2 makes its nucleation process autonomous; this differentiates iodine species from the sulphuric acid nucleation, which typically requires additional base molecules such as ammonia and amines to form stable clusters.[15,36] Importantly, the particle formation rates of iodine oxoacids (HIO_3 and HIO_2) exceed those of sulphuric acid at comparable acid concentrations, especially in the remote areas under low base concentrations.[16] The stabilising effect of HIO_2 was also seen with sulphuric acid.[21,37,38]

Since iodine oxoacid nucleation is a recently discovered mechanism, there exists a critical knowledge gap regarding the factors that influence nucleation rates in this chemical system. These factors include atmospheric ionisation rates, humidity, and temperature. The importance of atmospheric ionisation rates lies in their direct influence on particle formation dynamics, particularly in the upper troposphere where charged clusters play a significant role. Similarly, temperature is a crucial parameter affecting formation rates, as variations in temperature can significantly impact the stability and reactivity of precursor molecules.[39] Hence, understanding the precise influence of these factors is paramount for accurately representing them in models.

In this study, we carry out particle formation experiments at the CLOUD chamber at CERN aiming to improve the understanding of iodine oxoacid particle formation and its dependency on temperature, humidity and ionisation rate. As water vapour is a key component in the formation of iodic acid, varying the humidity may alter the ratio between iodine oxides and oxoacids. This may further allow us to disentangle the contribution of iodine oxoacids and oxides to iodine particle formation in the marine boundary layer. Additionally, we use a kinetic model to calculate the formation rate of charged iodic acid clusters at different temperatures, ionisation rates and sink. Recent measurements of iodine in the upper troposphere suggest the presence of HIO_3 in this region.[40] Combining those parameters allows us to evaluate how significant the charged cluster formation mechanism of iodic acid is in the upper troposphere.

2 Methods

2.1 CLOUD chamber

The data used in this study were collected during the CLOUD12 and CLOUD13 campaigns (2017 and 2018) at the Cosmics Leaving OUtdoor Droplets (CLOUD) chamber at CERN in Geneva, Switzerland. The CLOUD chamber is a 26.1 m^3 stainless

steel cylinder suitable for studying nucleation processes under well-controlled, atmospherically relevant conditions.[15,41]

We used three different ionisation settings to investigate the effect of ions on nucleation. First, the chamber was in the so-called neutral mode, in which a high-voltage field was used to remove all ions. Two electrodes created an electric field of up to 30 kV m^{-1}, thereby effectively removing all the ions inside the CLOUD chamber. When the electric field was turned off, ions were created in the chamber by natural galactic cosmic rays (GCRs). The ion production rate under such GCR conditions inside the chamber was determined to be 4.1 ion pairs cm^{-3} s^{-1}.[39] In the last setting, the chamber was exposed to a 3.5 GeV/c pion beam from the CERN Proton Synchrotron. This increased the ion production rate by approximately a factor of twenty compared to the GCR conditions.[39]

In this work, we focus on the nucleation experiments initiated by molecular iodine (I_2). During the experiments, stable concentrations of I_2 and ozone were maintained inside the chamber. We initiated each nucleation event by turning on the green light (528 nm), which photolysed I_2 to produce iodine atoms. Iodine atoms undergo oxidation processes which eventually form HIO_3 and HIO_2. Each nucleation experiment was continued until a steady state for each ionisation setting was reached, after which the chamber was cleaned and prepared for the next experiment.[16]

The experiments relevant to this study were conducted at both −10 °C and +10 °C. An additional series of experiments was carried out at +10 °C, with relative humidity (RH) ranging from below 0.008% to 80%. The cryogenic synthetic air employed in this investigation comprises 21% O_2 and 79% N_2, with a certified water concentration well below 1 ppmv (0.008% RH). To regulate humidity in the chamber, the primary airflow is humidified using a temperature-controlled Nafion humidifier, which utilises ultrapure water. In order to achieve the driest conditions possible for the experiments without added water vapour, the chamber was purged with cryogenic air for over a week before the dry experiments.

2.2 Instruments

Several instruments continuously monitored the experiments in the CLOUD chamber. The particle size distribution between 1 and 3 nm was measured with a scanning particle size magnifier (PSM) coupled with a condensation particle counter (CPC). The PSM is an aerosol pre-conditioner, which uses DEG (diethylene glycol) to grow aerosol particles as small as 1 nm to sizes that are easily detectable by a CPC.[42] The particles between 6 and 65 nm were measured with a nano scanning mobility particle sizer (nano-SMPS 3982, TSI),[43] while the particles larger than 65 nm were measured with a custom-built long SMPS. Additionally, a condensation particle counter (CPC) (TSI 3756) measured the total particle concentration above 2.5 nm. With these instruments, the particle size distribution from 1 nm to 1 μm was measured. The ion size distribution between 0.8 and 40 nm was measured by a Neutral Cluster and Air Ion Spectrometer (NAIS).[44]

Gas-phase species were measured using a nitrate chemical ionisation mass spectrometer (nitrate-CIMS) and a bromide-CIMS. The nitrate-CIMS is an APi-TOF (Atmospheric Pressure interface Time-Of-Flight) coupled with a chemical ionisation unit using nitric acid as the reagent gas. It is used extensively for detecting sulphuric acid, highly oxygenated organic molecules, and iodic acid (HIO_3). In this study, it was used to analyse the concentrations of HIO_3, HIO_2, I_2O_4 and I_2O_5. The details of the nitrate-CIMS instrument in this study can be found in Kürten *et al.* (2014).[45] The nitrate-CIMS has an ion filter integrated into its sampling line to separate ions and charged clusters from the neutral molecules; thus, it measures only neutral molecules and clusters in CLOUD. In this study, a bromide-CIMS was used to measure the water content in the chamber.[46] It is an APi-TOF coupled with a chemical ionisation unit using dibromomethane (CH_2Br_2) as the reagent gas. The CH_2Br_2 is fed into the sheath flow of the inlet, under the illumination of a soft X-ray source, producing bromide anions (Br^-). The Br^- ions are directed into the sample flow by a negative electric field, which then cluster with neutral molecules in the sample air.[46,47] With the measured water content using the H_2OBr^-,[46] we estimated the relative humidity below 2% in the chamber during the dry experiments. The detection limit in this case is inadequate for measuring the water content in the dry cryogenic air. Nonetheless, it serves the purpose of ensuring that no unintended humidity is introduced into the cryogenic air. Above 2% the relative humidity was measured using the dew point monitor DewMaster from EdgeTech. We chose a time when both the dew point monitor and the bromide-CIMS were working well to calculate a calibration factor, which we then used to estimate the humidity below 2%.

2.3 Field observations in the Arctic

In this study, iodine oxoacid particle formation rates from the CLOUD experiments are compared to field observations by Baccarini *et al.* (2020)[24] who reported new particle formation events during the Arctic Ocean expedition between August and September 2018. The authors found that the observed particle formation events were predominantly driven by iodine species. HIO_3 and H_2SO_4 were measured using a nitrate-CIMS. We used the combined particle size distribution (2.14–921 nm) measured with an NAIS and a custom-built differential mobility particle sizer (DMPS) from that study to calculate the particle formation rate. Further details about this field campaign can be found in Baccarini *et al.* (2020).[24]

We calculated the formation rate at 2.5 nm ($J_{2.5}$) for five event days, where the HIO_3 concentration was between 1×10^6 and 8×10^6 cm^{-3} and the temperature between 0 and −10 °C. The sulphuric acid and methanesulphonic acid concentrations were negligible (below 7×10^5 cm^{-3} and 4×10^5 cm^{-3} respectively) during the events. The standard deviation was calculated for the $J_{2.5}$ and the HIO_3 concentration to estimate the uncertainty.

2.4 Formation rates

The formation rate of aerosol particles (J_{D_p}) is defined as the flux of particles above a certain particle diameter D_p, which is 1.7 nm in this study. For chamber measurements, the formation rate was calculated by taking the derivative of the total

concentration measured above 1.7 nm (dN/dt) and accounting for the size-dependent losses of particles due to dilution S_{dil}, wall loss S_{wall} and coagulation loss S_{coag}.

$$J_{1.7} = \frac{dN_{>1.7}}{dt} + S_{dil} + S_{wall} + S_{coag} \quad (1)$$

A more detailed description of the formation rate calculation can be found in Dada *et al.* (2020).[48] The formation rate of each experiment was determined as the median value after reaching a steady state.

For field measurements, a different size range had to be used due to limited instrumentation. The formation rates were calculated for a specific size range (from 2.5 to 25 nm in this study), instead of the total particle population above a certain size, because it is possible that other particle sources could contribute to the particle population, especially at larger sizes. In addition, while wall and dilution losses are not applicable for the atmosphere, freshly formed particles can grow out of the size range (*i.e.*, 25 nm), therefore the loss due to growth out of the size range needs to be accounted for (S_{GR}). Finally, the particle formation from the Arctic field study can be calculated using the following equation:[49]

$$J_{2.5} = \frac{dN_{2.5-25}}{dt} + S_{coag} + S_{GR} \quad (2)$$

The formation rates were averaged from the beginning of the new particle formation event until its peak. The growth rates ($GR_{5-20\ nm}$) were calculated by Baccarini *et al.* (2020)[24] for the mean diameter mode of the events. Both for the chamber experiments and the field observations, the standard deviation was calculated to represent the errors.

2.5 Definitions

In the following paragraph, we will clarify the formation rate terminology used in this publication. We use the same definitions as Wagner *et al.* (2017).[50] The total formation rate, J_{tot}, consists of the neutral formation rate, J_N, which can be measured during the neutral stages of CLOUD experiments (see Section 2.1), and the ion-induced formation rate, J_{iin}, which in turn consists of the formation rate of the charged ion clusters, $J_{\pm}$, and the formation of neutral clusters due to ion–ion recombination, J_{rec}.[51] Thus, the total formation rate can be written as:

$$J_{tot} = J_N + J_{\pm} + J_{rec} \quad (3)$$

At CLOUD we can directly measure J_N, J_{GCR}, and J_{Beam} by varying the ionisation setting of the chamber between Neutral, GCR and Beam, as explained in Section 2.1. During the Neutral stage, we can directly measure J_N and during the GCR and Beam stages, we can measure J_{tot} at different ionisation rates. Therefore, J_{iin} can be calculated with

$$J_{iin} = J_{GCR} - J_N \quad (4)$$

This requires that all the experimental conditions except the ionisation rate stay the same. A time series of the formation rate during a CLOUD experiment is plotted in Fig. 1 to visualise the terms contributing to nucleation at different stages of the experiment. In order to disentangle $J_{\pm}$ from J_{iin}, the PANDA520 model[16,52] was used to simulate the formation rate of charged clusters $J_{\pm}$ at 1.7 nm. We note that $J_{\pm}$ differs from J_{iin} because the model does not factor in neutralised particles resulting from ion–ion recombination.

2.6 PANDA520 model

The kinetic model Polar ANd high-altituDe Atmospheric research 520 (PANDA520)[52] was used to calculate the formation rate of the charged clusters ($J_{\pm}$) for ion-induced iodic acid nucleation. Further information on the model can be found in He *et al.* (2021).[52] For this study, the PANDA520 model was simplified to only include the parametrisations that are necessary for this study, which are wall and dilution loss, ion–ion recombination and ion–neutral collision processes. Additionally, we included temperature and pressure dependent parametrisations to investigate the temperature and altitude dependency of the formation rate of charged clusters.

It was previously shown that ion-induced iodic acid nucleation only occurs in the negative ion channel, while the positive ion channel shows no cluster growth.[16] Therefore, positive clusters are treated as one of the sinks for the negative clusters in the model. Additionally, evaporation rates are not taken into account in the model since He *et al.* (2021)[16] has concluded that ion-induced nucleation from iodine oxoacids proceeds at the collision limit with negligible cluster evaporation, specifically at temperatures below 10 °C. Furthermore, the model includes parametrisations for wall and dilution loss, ion–ion recombination and ion–neutral collision.

The wall loss is calculated based on the equation from Crump *et al.* (1981)[53] and takes the temperature, pressure, and particle diameter into account.[52] The dilution loss is 1.6×10^{-4} s^{-1}, which is calculated from the volume and the total flow of the CLOUD chamber; 26.1 m^3 and 250 litre per minute respectively. In the simulations for atmospheric conditions, the wall loss is used to mimic the sink of charged clusters to large particles in the atmosphere (coagulation loss) and wet and dry deposition.

The ion–ion recombination rate (k_{rec}) was calculated according to the parametrisation from Israël (1957)[54] which takes the pressure and temperature into account. According to Zauner-Wieczorek *et al.* (2022),[55] this parametrisation has the best agreement with field and model data for an altitude range of 0–22 km. We calculated the ion–ion recombination rate for the upper troposphere by adjusting the temperature and pressure according to the international standard atmosphere,[56] which is a standardised model of the vertical temperature and pressure changes.

The ion–neutral collision rates and negative ion transfer rates were calculated with the tool provided by Kummerlöwe *et al.* (2005).[57]

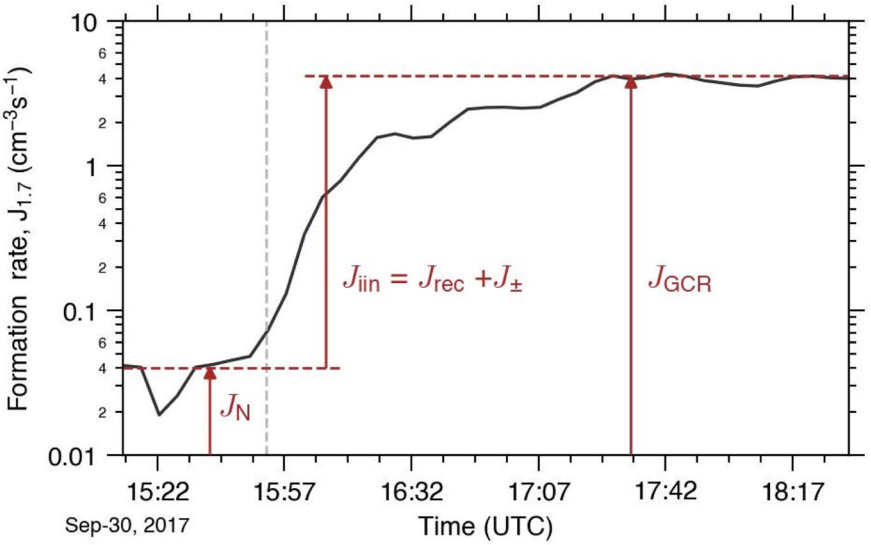

Fig. 1 An example of the formation rate time series at different ionisation settings to visualise the terminology used in this study. In the first stage of the experiment, the HV clearing field was turned on to establish ion-free conditions in the chamber and thus we measured the neutral formation rates (J_N). At the end of this stage (15 : 50, indicated with a vertical dashed line), the HV clearing field was switched off. After this point, the ions produced by galactic cosmic rays (GCRs) were no longer removed from the chamber and the particle formation rates increased (J_{GCR}). The difference between J_{GCR} and J_N represents the ion-induced formation rate (J_{iin}).[50]

The ionisation rate (IR) for most of the modelled results in this simulation was set to 4.1 ion pairs cm^{-3} s^{-1}, based on steady-state concentrations of ions in the CLOUD chamber. Additionally, we used ionisation rates of 10, 20 and 50 ion pairs cm^{-3} s^{-1} to investigate the influence of the ion production rate on the formation rate of charged clusters. We chose 50 ion pairs cm^{-3} s^{-1} as the maximum value because it represents the ionisation rate in the atmosphere at around 15 km.[58]

The formation rate of the charged clusters can be calculated as shown here:

$$J_{\pm} = N^{-}_{\mathrm{crit}-1}[\mathrm{HIO_3}]k_{\mathrm{col}} \quad (5)$$

$[HIO_3]$ is the iodic acid concentration and k_{col} is the collision rate. N^{-}_{crit} is the concentration of the negative ion cluster concentration at the selected size, which is 1.7 nm in this study. We need to know how many monomers are needed for a cluster to reach the selected size. Under the assumption that the monomers are spherical, we can calculate this number with eqn (6):

$$d_p = \left(\frac{6 \cdot i \cdot M}{\pi \cdot N_A \cdot \rho}\right)^{\frac{1}{3}} + 0.3\ \mathrm{nm} \quad (6)$$

where M is the molecular mass and ρ is the density of HIO_3 monomer. The density was determined by R'Mili *et al.* (2022)[59] to be 2.83 g cm^{-3} at 22% relative humidity. N_A is the Avogadro constant and we add 0.3 nm for the mobility correction (difference between mass and mobility diameter).[60] The number of monomers needed to reach the selected size (1.7 nm) is represented by *i*. After accounting for the 0.3 nm mobility shift, 14 iodic acid monomers are needed to reach the selected cluster size of 1.7 nm. Additionally, we also calculated the diameter under the assumption that each iodic acid molecule contains two water molecules.[16] This is a more realistic approach since charged iodine clusters are usually hydrated in the atmosphere.[61] In this case 10 monomers are needed to reach the selected cluster size of 1.7 nm. We use this in Section 3.3, where we compare the model data with the field and CLOUD data.

3 Results

3.1 Experimental formation rates at different temperatures and ionisation rates

A typical series of iodine oxoacid nucleation experiments at +10 °C (panel 2A) and at −10 °C (panel 2B) in the CLOUD chamber are shown in Fig. 2. The upper panel shows the total formation rates and the ion concentrations during the experiments, the middle panel shows the HIO_3 and HIO_2 concentrations, and the bottom panel shows the particle size distribution measured by the SMPS. The dotted line separates the different stages of the experiment, in which the chamber was either in the Neutral, GCR or Beam modes (see Section 2.1). Iodine (I_2), ozone and water were added to the chamber during the experiments. Subsequently, I_2 was photolysed and oxidised to form HIO_3 and HIO_2.[16,32] The concentrations of HIO_3 and HIO_2 and other experimental conditions, except the ionisation rate, were kept stable during this set of experiments, so any change in the formation rate can be attributed solely to the change in ionisation rate.

When comparing panels A and B, it is apparent that the formation rate increases significantly when the temperature decreases. The average HIO_3 and HIO_2 concentrations are 2×10^7 cm^{-3} and 5×10^5 cm^{-3} at +10 °C (A2) and 8×10^6 cm^{-3} and 2×10^5 cm^{-3} at −10 °C (B2). Even with the lower concentration of iodine oxoacids, the neutral particle formation rate at −10 °C exceeds that at +10 °C by approximately two orders of

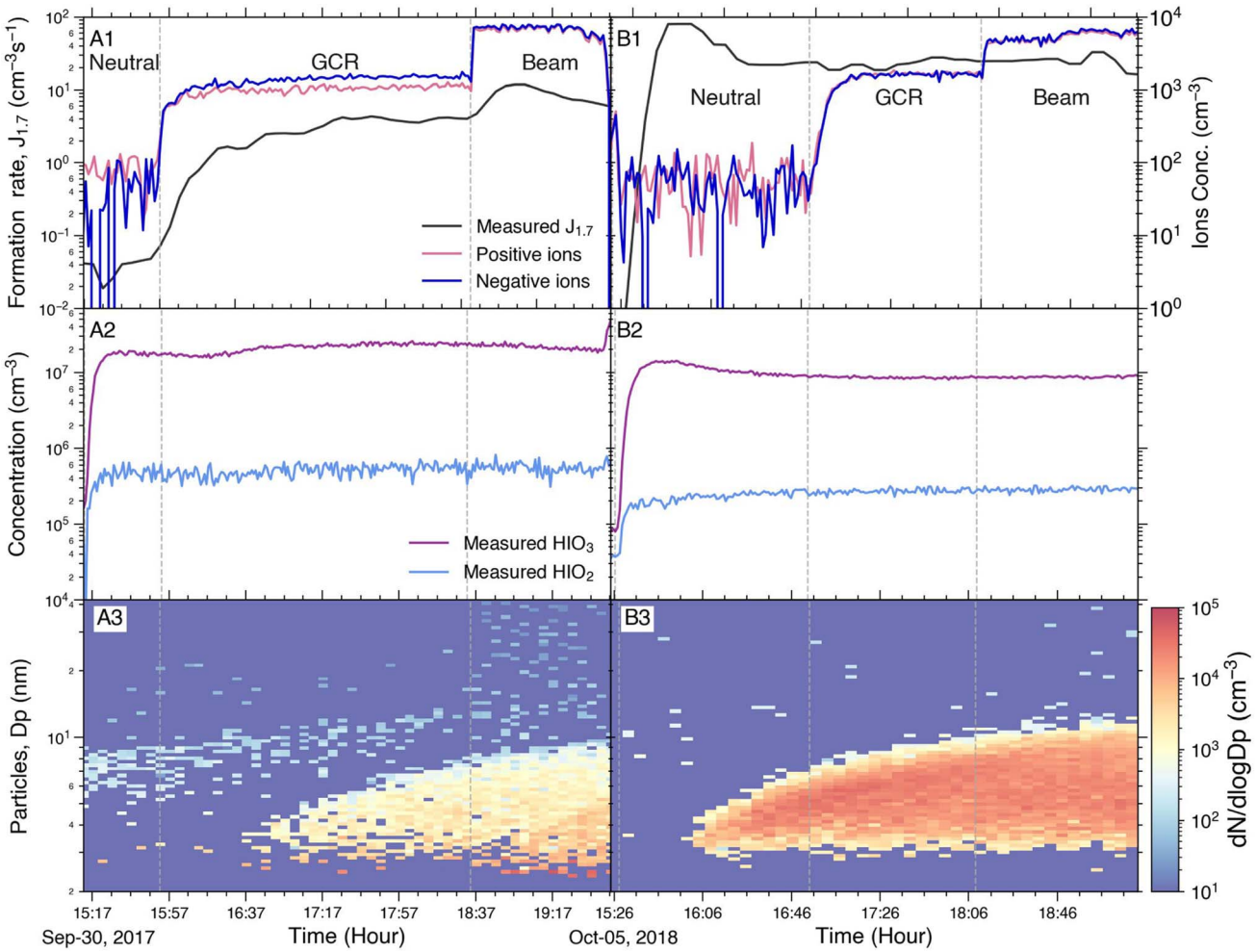

Fig. 2 Iodine oxoacid nucleation in the CLOUD chamber at +10 °C (panel A) and −10 °C (panel B). The plots show the calculated formation rate at 1.7 nm and the total ion concentration measured by the NAIS in the top panels (A1 and B1). The second panels (A2 and B2) show the HIO_3 and HIO_2 concentrations and the third panels (A3 and B3) show the particle size distribution measured by the SMPS. The formation rate increases from +10 °C to −10 °C. Furthermore, the ion enhancement is clearly visible at +10 °C whereas there is no significant change at −10 °C. This shows that neutral nucleation dominates the formation process at −10 °C.

magnitude. This confirms that a lower temperature significantly enhances the neutral iodine oxoacid nucleation, consistent with previous studies.[16,62,63] The temperature enhancement can be seen as well in the particle size distributions (A3 and B3); the latter clearly features a stronger formation rate.

Furthermore, the ion enhancement of the formation rate is clearly visible at +10 °C (A1), whereas at −10 °C there is no significant change in the total formation rate when the ionisation rate is changed (B1). This is likely due to the fact that ion-induced nucleation of iodic oxoacids is already proceeding at the kinetic limit at +10 °C and therefore cannot increase further when the temperature decreases.[16] On the other hand, the neutral iodine oxoacid nucleation is relatively weak at +10 °C and it is significantly enhanced at −10 °C. Hence, the neutral iodine oxoacid nucleation dominates the total formation rate at −10 °C and the ion-induced channel becomes less significant. In contrast, elevating the ionisation rate from 0 to 4.1 ion pairs cm^{-3} s^{-1} at +10 °C results in an increase of the formation rate from 0.04 to 3.5 cm^{-3} s^{-1}, highlighting the importance of ion-induced nucleation at warmer temperatures. Interestingly, increasing the ionisation rate further from GCR conditions to Beam-enhanced conditions increases the formation rate only by a factor of 2 from 3.5 to 7.2 cm^{-3} s^{-1}. This differentiates the iodine oxoacid nucleation from, *e.g.*, the sulphuric acid–ammonia system in which a larger beam enhancement was observed.[15] As ion-induced nucleation is thought to have potential climate impacts especially in the upper troposphere–lower stratosphere,[15,64] resolving the ionisation rate enhancement is crucial. We will investigate this phenomenon in the following section.

3.2 Modelling charged cluster formation rates at different altitudes

We use the PANDA520 model[52] to investigate the impact of changing environmental conditions on the formation rate of the charged HIO_3 clusters, $J_{\pm}$. While our previous studies

mainly focused on marine boundary layer conditions,[16,52] we have extended the parametrisation in this study to cover conditions from the marine surface to lower stratospheric conditions (see Methods). In Fig. 3, we examine the dependency of $J_{\pm}$ on temperature, ionisation rate, and the sink (a surrogate for coagulation sink, dry deposition, wet deposition, *etc.*).

The model shows that $J_{\pm}$ only has a very weak temperature dependence, being slightly lower at lower temperatures (Fig. 3A), which is due to the fact that the recombination loss increases with decreasing temperature. Therefore, more ions will be lost due to ion–ion recombination processes. This confirms the conclusion that the temperature dependence of J_{tot}, which was seen in Fig. 2, comes from the neutral nucleation pathway, which is strongly enhanced by a lower temperature.

In contrast, the ionisation rate has a clear effect on $J_{\pm}$ (Fig. 3B). At high iodic acid concentrations, a higher ionisation rate leads to higher formation rates. But interestingly, when the iodic acid concentration is lower than about 1.5×10^7 cm^{-3}, increased ionisation rate suppresses $J_{\pm}$. This goes against the general conception that an increased ionisation rate always leads to an enhanced formation rate.[15,36] This is because higher ionisation rates result in elevated ion concentrations. However, the higher ion concentrations also lead to increased recombination losses between ions of opposite charge. The higher ionisation rate enhances the total ion concentration essentially linearly. On the other hand, the survival probability of an ion monomer (*i.e.*, IO_3^-) growing to 1.7 nm relies on the growth by sequential HIO_3 additions and the sink by neutralisation with cations. It should be noted that the neutralisation process affects every step of the cluster growth process. Hence, the heightened total ion concentrations and the diminished cluster survival probability exhibit distinct dependencies on the ionisation rate. When a certain level of iodic acid is reached, the gain of 1.7 nm ions due to condensational growth outweighs the loss of ions due to recombination and $J_{\pm}$ increases with the increasing ionisation rate. However, at low to moderate iodic acid concentrations, this dependence will be reversed. The same principle applies to charged particle coagulation loss to larger charged particles of opposite polarity.[65] Our data show that the turning point for HIO_3 is at approximately 1.5×10^7 cm^{-3}. This explains, at least partly, why the beam enhancement in the experiment presented in Fig. 2 A1 ($HIO_3 = 2 \times 10^7$ cm^{-3}) is rather weak.

Finally, the sink due to larger particles (coagulation loss) and deposition has the expected effect of decreasing the formation rate (Fig. 3C). The default sink value used in the simulations at +10 °C is 0.002 s^{-1} which originates from the wall loss rate of CLOUD.[52] It is important to note that increasing the sink from its default value has a more significant impact on overall formation rates compared to decreasing the sink by the same factor at HIO_3 <2×10^7 cm^{-3}. This is because the charged cluster formation process is controlled by two major sinks in the atmosphere: ion–ion recombination and coagulation with existing neutral particles. Neither of these processes depends on the concentration of HIO_3. Conversely, the charged cluster growth process is dominated by HIO_3 condensation. Therefore, at lower HIO_3 concentrations, increasing the sink would have a more significant impact on reducing the cluster formation rate.

In order to estimate the collective impact of these parameters and to explore the potential significance of $J_{\pm}$ across different altitudes of the marine atmosphere, we utilised the conditions stipulated by the international standard atmosphere.[56] This allowed us to adjust the temperature and pressure in accordance with prescribed values and subsequently compute the formation rate at various altitudes (depicted in Fig. 4). At the sea level (0 km), the pressure and temperature stand at 1013 hPa and 15 °C, respectively. At 5 km, these values change to 540 hPa and −17.5 °C; at 10 km, they are 264 hPa and −50 °C; and at 15 km, they reach 120 hPa and −56.5 °C. As

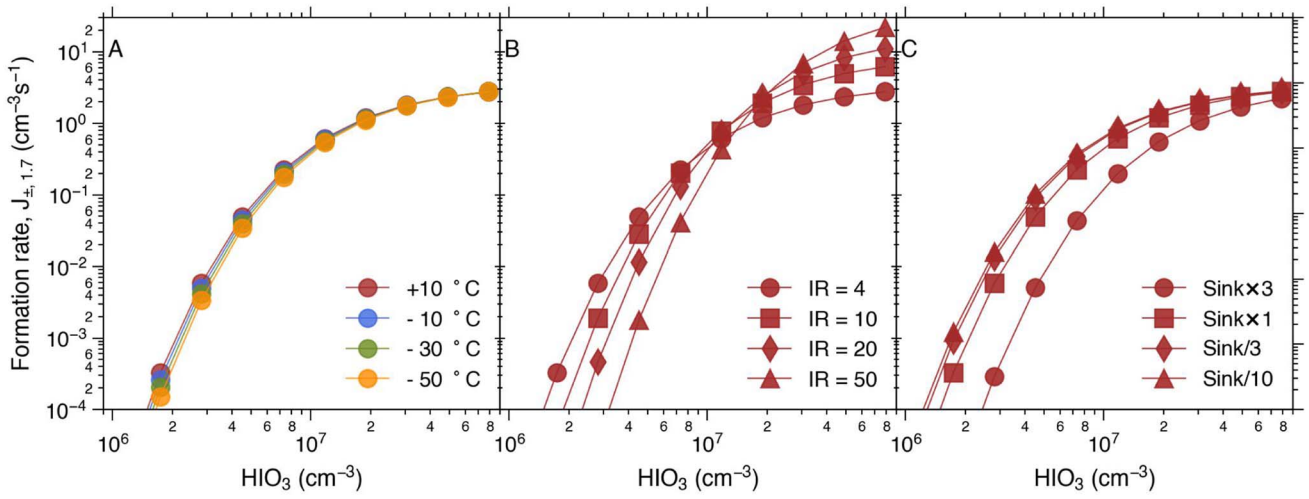

Fig. 3 The temperature (A), ionisation rate (B), and sink (C) dependence of $J_{\pm}$ simulated by the PANDA520 model. If not stated otherwise the temperature is +10 °C, the ionisation rate is 4.1 ion pairs cm^{-3} and the sink is 0.002 s^{-1}. This shows that from these three parameters, the charged cluster formation rate is most sensitive to the ionisation rate. At HIO_3 concentrations below 1.5×10^7 cm^{-3} the impact of recombination loss is higher than the ion growth due to HIO_3 condensation and the formation rate decreases with increasing ionisation rate.

altitude increases, both temperature and pressure decrease, while the ionisation rate due to galactic cosmic rays increases. Additionally, in Fig. 4B, we introduced variation to the sink, simulating its highest magnitude at the ground level and subsequent decrease at higher altitudes.

The ionisation rate has the greatest influence on $J_{\pm}$ across the range of altitudes simulated here. At low HIO_3 concentrations, the increasing ionisation rate at higher altitudes leads to a decreased $J_{\pm}$, whereas the opposite is the case at high HIO_3 concentrations (>1.5×10^7 cm^{-3}, Fig. 4A). In Fig. 4B, the sink is also considered, which decreases the formation rate, especially at the lowest altitudes and thus evens out the simulated formation rates at different parts of the atmosphere. Since the HIO_3 concentration in marine atmospheres (excluding the coastal regions) is likely close to or below 1×10^7 cm^{-3},[16,40] the low HIO_3 concentrations are likely mechanistically more interesting.

All in all, our results indicate that enhancing the ionisation rate may not necessarily accelerate new particle formation since it is also dependent on the chemical system. One unique thing about ion-induced HIO_3 nucleation is that it proceeds at the collision limit at temperatures of +10 °C and below, *i.e.*, every collision of HIO_3 with charged clusters leads to irreversible growth,[16,52] which is not the case for systems such as sulphuric acid and oxidised organic vapours. Hence, in the case of the iodic acid system, a threshold of 1.5×10^7 cm^{-3} is observed, beyond which increased ion concentrations result in higher rates of charged cluster nucleation. It is important to note that different systems may exhibit varying thresholds.

Our results further indicate that ion-induced nucleation probably does not play a significant role in iodine oxoacid particle formation in the upper troposphere–lower stratosphere, where the low temperatures favour the neutral iodine oxoacid nucleation, and the formation rate of charged clusters ($J_{\pm}$) is low according to our simulations. It has to be noted that our model only considers the charged clusters that survive until the critical size, and does not consider the possible enhancement of ion-induced nucleation by ion–ion recombination processes. However, we expect that the combined change of $J_{\pm}$ and J_{rec} (*i.e.*, J_{iin}) is still insignificant compared to the enhancement of neutral formation rate at lower temperatures. This is supported by Fig. 2, as panel B1 clearly shows that the

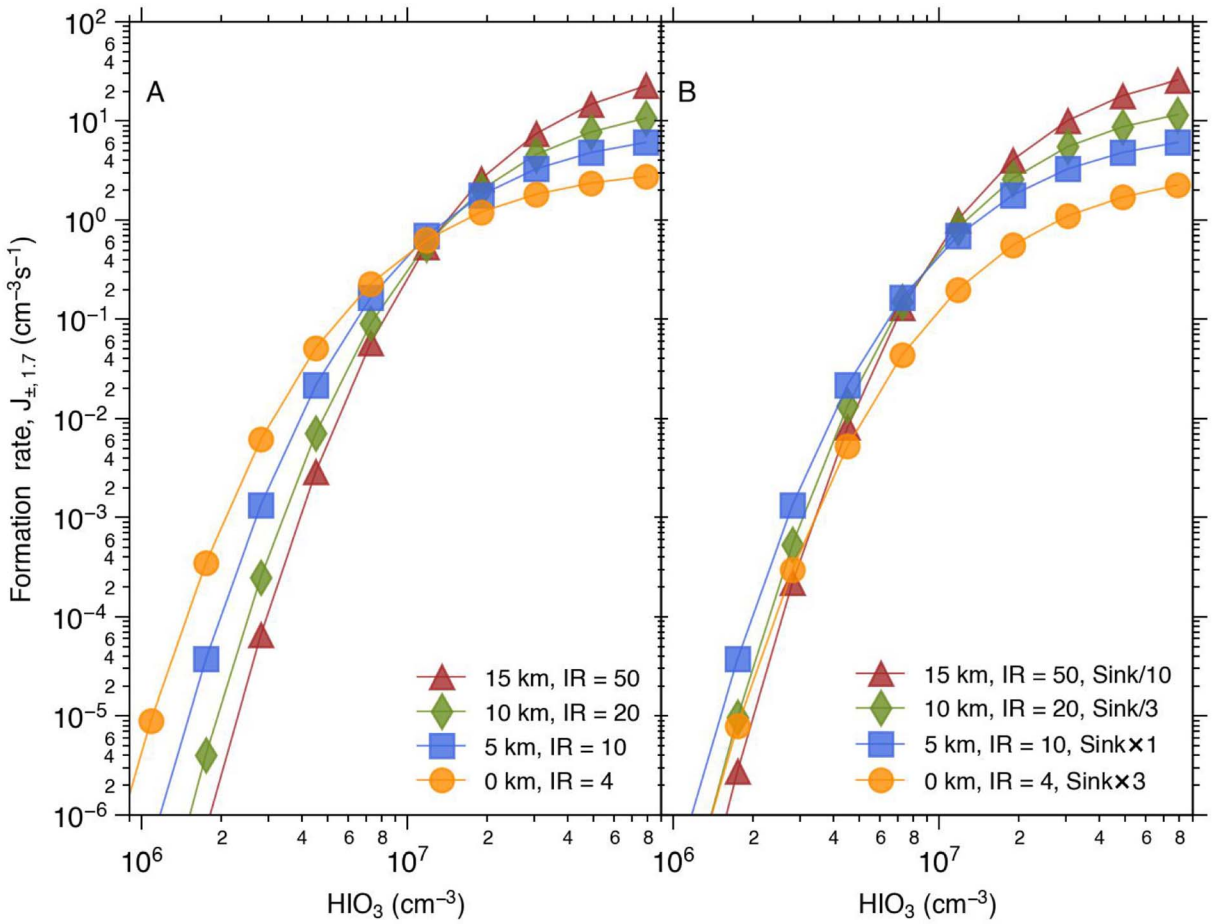

Fig. 4 The simulated formation rate of charged clusters under conditions representing different altitudes. The pressure and temperature were adjusted according to the international standard atmosphere[56] and the ionisation rate increases with increasing altitude (A). The pressure and temperature at the different altitudes are 1013 hPa and 15 °C at 0 km; 540 hPa and −17.5 °C at 5 km; 264 hPa and −50 °C at 10 km and at 15 km it is 120 hPa and −56.5 °C. In figure (B) the sink effect is added.

increase in ionisation rate has minimal effect on the total formation rate (J_{tot}) at −10 °C. This may well extend to lower temperatures as neutral J_N will likely be further enhanced at lower temperatures while J_{iin} changes moderately.

On the other hand, it is also clear from our data that ion-induced nucleation can significantly enhance particle formation rates from HIO_3 at temperatures above 0 °C and iodic acid concentrations below about 5×10^7 cm^{-3},[16] which makes the ion-induced nucleation mechanism important in large parts of coastal and marine lower atmospheres.

3.3 Comparison between model, laboratory data and field observations

We verified the model used in this study by comparing the formation rate of charged clusters ($J_\pm$) to the formation rates determined from CLOUD experiments (J_N and J_{GCR}) in Fig. 5. The lower limit of the shaded area shows the simulated $J_\pm$ at +10 °C, in which we assume that the condensing monomer is HIO_3, and the upper limit shows the same for $HIO_3 + 2H_2O$ being the condensing monomer. The measured J_{GCR} at +10 °C are close to the modelled $J_\pm$ below an HIO_3 concentration of about 5×10^7 cm^{-3}. This good agreement indicates that $J_\pm$ dominates the J_{tot} (J_{GCR}) under these conditions. Our earlier study[16] has confirmed a negligible J_N under these conditions. Thus, this good agreement indicates that $J_\pm$ dominates the J_{tot} (J_{GCR}). However, due to uncertainties of our experiments and model, we cannot distinguish a J_{rec} contribution of up to 50% of the J_{tot}. Therefore, we do not exclude the possibility of a minor contribution from J_{rec}. At higher HIO_3 concentrations J_N increases rapidly, while $J_\pm$ levels off because it is limited by the ion production rate and therefore, J_{GCR} starts to deviate from the model line.

Finally, we compare iodine oxoacid formation rates from CLOUD and model data to field observations. The challenge is that it is difficult to find field data with necessary instrumentation and where we can safely assume that the nucleation and early growth are dominated by iodine oxoacids, since very often other potential precursor vapours such as sulphuric acid, methanesulphonic acid and/or various organic compounds are present simultaneously.[25] However, Baccarini *et al.* (2020)[24] reported observations of new particle formation driven by iodic acid in the central Arctic Ocean. We used the data from Baccarini *et al.* (2020)[24] to calculate $J_{2.5}$ for a subset of reported particle formation events, where particles were present in the smallest size channels of the NAIS so that we could assume that they were formed at or very close to the measurement location (Fig. 5, triangle symbols). It was not possible to calculate $J_{1.7}$ directly, since no instruments that measured this size range were present. Given the uncertainties in the instrumentation, slightly different size range ($J_{2.5}$ is commonly smaller than $J_{1.7}$) and method to calculate the formation rates (see Section 2.4), we consider that the

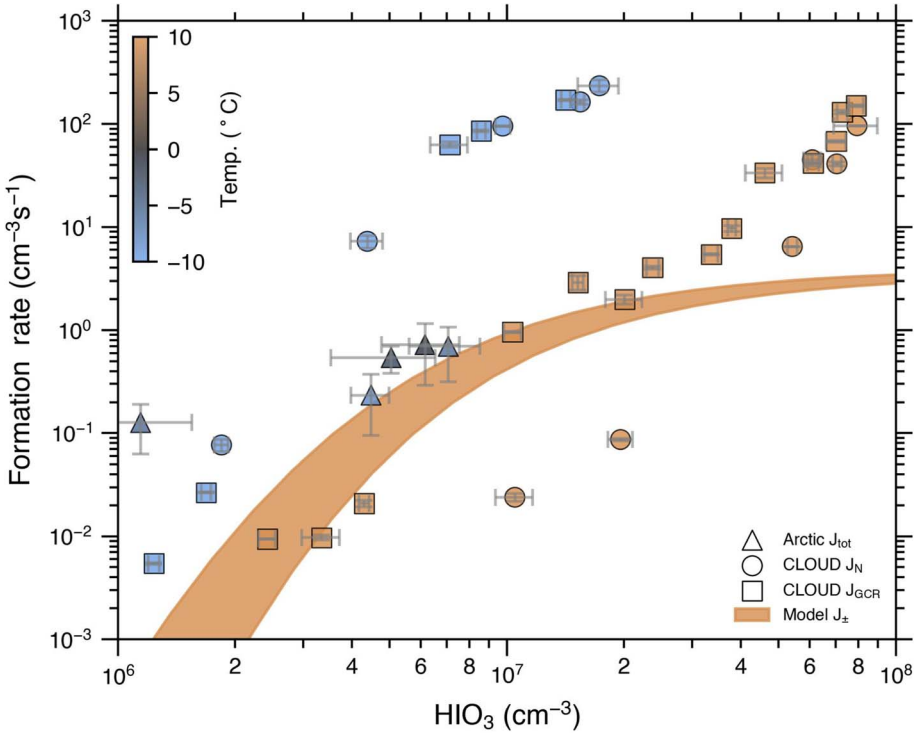

Fig. 5 Total formation rate, J_{tot} at 1.7 nm from GCR and Neutral runs at CLOUD (same data as in He *et al.* (2021)[16]) compared to the charged cluster formation rates from the simplified PANDA model at +10 °C, as well as J_{tot} at 2.5 nm from field measurements in the Arctic Ocean.[24] The error bars are the standard deviation of the measurement data. Shaded area is the formation rate of charged clusters for HIO_3 clusters (lower limit) and $HIO_3 + 2H_2O$ clusters (upper limit) at 1.7 nm. The model data agree well with the CLOUD GCR points at +10 °C below 5×10^7 cm^{-3}, where the ion-induced nucleation dominates.

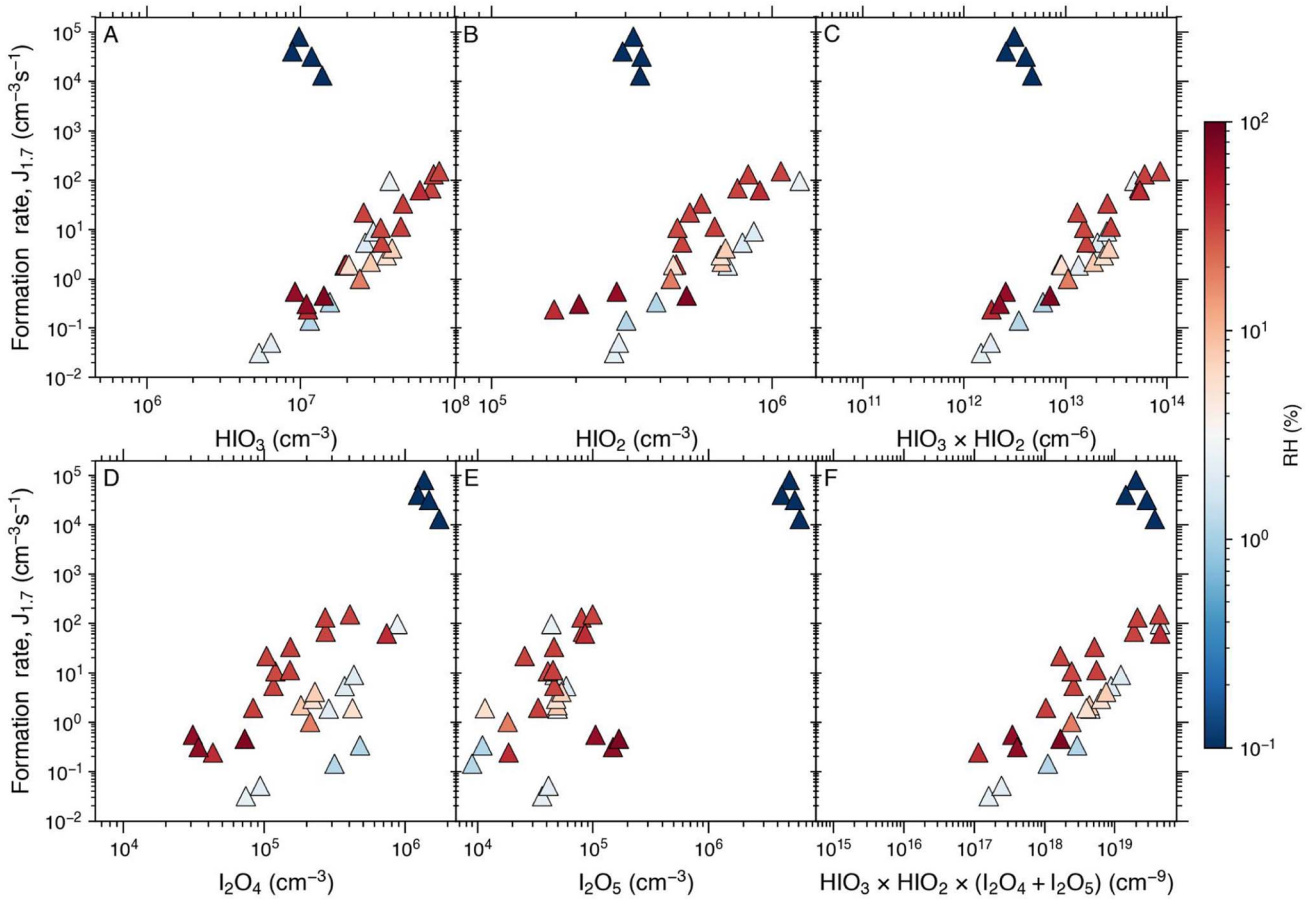

Fig. 6 Formation rates at different relative humidities (below 0.008 to 80%) in the CLOUD chamber under GCR conditions at +10 °C against different iodine compounds: (A) HIO_3, (B) HIO_2, (C) $HIO_3 \times HIO_2$, (D) I_2O_4, (E) I_2O_5 and (F) $HIO_3 \times HIO_2 \times (I_2O_4 + I_2O_5)$. The iodine species are measured with the nitrate-CIMS. It can be seen that the formation rate is largely unaffected by the changing humidity, but at extremely low humidity (not relevant for the troposphere and stratosphere), it increases by two orders of magnitude probably due to the contribution of high I_2O_4 and I_2O_5.

agreement is reasonable. The observed particle formation rates in the Arctic Ocean at temperatures from −1 °C to −9 °C fall mostly between the CLOUD data at +10 °C and −10 °C, and a little bit above the simulated $J_{\pm}$. This is in agreement with the interpretation of Baccarini *et al.* (2020)[24] that particle formation during the reported events proceeds as negative ion-induced iodic acid nucleation, with a potential contribution from the neutral channel as well.

3.4 Humidity dependence of formation rates and mechanism

Finally, we investigated the humidity dependence of iodine particle formation rates and mechanisms under GCR conditions by adjusting the amount of water vapour in the CLOUD chamber. These experiments were conducted at +10 °C and relative humidity from below 0.008% to 80%, which is equivalent to an absolute water molecule concentration of 2.52×10^{13}–2.55×10^{17} cm^{-3}. In Fig. 6, the total particle formation rates are plotted against different iodine species that possibly participate in the clustering process (*i.e.*, HIO_3, HIO_2, I_2O_4, and I_2O_5) and combinations of them ($HIO_3 \times HIO_2$, $HIO_3 \times HIO_2 \times (I_2O_4 + I_2O_5)$) to investigate the key nucleating species under different relative humidity conditions.

For RH >2%, iodine oxoacid particle formation has no obvious dependence on RH. This feature is distinct from the nucleation processes from sulphuric acid and oxidised organic vapours, where a strong RH dependence has been observed.[39,66] Also, J_{tot} can be almost perfectly constrained by iodine oxoacid concentrations (Fig. 6A–C), consistent with the results from our previous studies.[16,35] This holds both at low HIO_3, where ion-induced nucleation mechanisms dominate, and at high (>5×10^7 cm^{-3}) HIO_3 where neutral processes dominate, as shown in Section 3.3.

Interestingly, the formation rates in the dry experiments behave very differently compared to the data points with RH >2%. These represent the driest reachable conditions in the CLOUD chamber with an RH of below 0.008% (or absolute water molecule concentration of 2.52×10^{13} cm^{-3}). Such extremely dry conditions are achieved by using certified cryogenic air which was used to purge the chamber for over a week before the dry experiments.[46] The particle formation rates observed in the dry experiments are much higher than in the other experiments

(Fig. 6) and these extremely high rates cannot be explained by the iodine oxoacid nucleation mechanism.[16,35] In the dry experiments, iodine oxide concentrations (*e.g.*, I_2O_4 and I_2O_5) are much higher, which suggests that dry conditions favour the formation of higher iodine oxide concentrations which leads to accelerated particle formation. However, it is important to emphasise that the water concentrations in the dry experiments are not representative of typical tropospheric conditions. Consequently, they are presented here solely as a mechanistic reference.

As soon as we introduced water vapour into the chamber (RH = 2%), I_2O_4 and I_2O_5 concentrations dropped sharply, especially the I_2O_5 concentration decreased by two orders of magnitude. This is expected since I_2O_5 reacts with water to form iodine oxoacids.[32] It should be noted that when the RH is higher than 2%, the I_2O_5 concentration is too low to be relevant for aerosol nucleation ($<2 \times 10^5$) and the I_2O_4 concentration is lower than the HIO_2 concentration. The potential role of I_2O_4 in iodine particle formation through, *e.g.*, HIO_3–I_2O_4 nucleation may be worth considering as I_2O_4 has been thought to be driving iodine particle formation.[28] However, our data indicate a minor contribution of I_2O_4 to iodine particle formation. First, the correlation between J_{tot} and I_2O_4 is clearly impacted by the RH since higher RH lowers the concentration of I_2O_4 while enhancing J_{tot} at the same time. This should be the opposite if I_2O_4 were to contribute to J_{tot} significantly.

The negative dependence of the I_2O_4 concentration on RH additionally suggests that its role in the marine boundary layer might be small. For example, at RH = 80%, the average I_2O_4 : HIO_3 and I_2O_4 : HIO_2 ratios are 0.005 and 0.146, respectively, and one may expect that these ratios may be even lower in the marine boundary layer with an RH frequently higher than 80%.

All in all, our results suggest that the iodine oxoacid nucleation is the dominant iodine particle formation mechanism in the marine and polar boundary layer for all relevant temperatures and humidities and that larger iodine oxides such as I_2O_4 and I_2O_5 play minor roles.

4 Conclusions

In this study, we used a combination of laboratory experiments and a kinetic model to investigate how new particle formation from iodine species depends on external conditions, such as temperature, humidity, and ionisation rate. This information is crucial for future inclusion of this newly found mechanism in global aerosol models.

A kinetic model (PANDA520) was used to simulate the charged cluster formation rate of iodic acid and its dependency on temperature, ionisation rate, and sinks. The results showed that the formation rate of charged clusters is not significantly dependent on temperature, but it is strongly dependent on the ionisation rate. $J_{\pm}$ increases with increasing ionisation rate, but only if the iodic acid concentration is above *ca.* 1.5×10^7 cm^{-3}. This is because with increasing ionisation rate, the ion concentration and therefore the recombination loss also increases. When the HIO_3 concentration exceeds 1.5×10^7 cm^{-3}, along with a higher ionisation rate, ion growth due to collisions increases more rapidly than recombination loss. This results in an elevated formation rate. The model results agreed both qualitatively and quantitatively with the chamber experiments at +10 °C. On the other hand, as the neutral nucleation of iodic acid is strongly dependent on temperature,[16] the neutral pathway became dominant at −10 °C and the total formation rate was insensitive to the ionisation rate.

This leads to the conclusion that despite higher ionisation rates, charged cluster nucleation of iodic acid is probably negligible at high altitudes with cold temperatures and low iodic acid concentrations. However, in the marine boundary layer, ion-induced iodic acid nucleation is important, as suggested also by the few existing field observations.[24]

The formation rates showed no dependence on relative humidity, as long as RH was above 2%. Therefore, the formation rates could be constrained by the iodine oxoacid mechanism ($HIO_3 \times HIO_2$) over a wide range of RH and acid concentrations. I_2O_4 and I_2O_5 play a significant role in the nucleation process, only if the atmosphere is extremely dry (below 0.008% at +10 °C). These desiccated conditions do not accurately represent tropospheric conditions. As a result, our findings suggest that the iodine oxoacid nucleation mechanism is the predominant pathway for iodine nucleation within the marine boundary layer atmosphere.

Data availability

The data have been made available on zenodo in the CERN CLOUD experiment community with the **https://doi.org/10.5281/zenodo.10797483**.

Author contributions

Resources, preparing the CLOUD facility and measuring instruments: B. R., X.-C. H., J. S., R. B., L. D., J. K., A. A., A. B., D. M. B., L. C.-P., H. F., H. L., C. P. L., V. M., H. E. M., G. M., R. M., A. O., M. P., W. S., M. Simon, D. S., Y. J. T., A. C. W., D. Wang, Y. W., M. W., S. K. W., M. Z.-W., J. C., I. E. H., R. C. F., T. P. and R. V. Data collection: B. R., X.-C. H., R. B., L. D., J. K., A. A., A. B., L. C.-P., J. D., H. F., H. L., C. P. L., G. M., R. M., B. M., M. Simon, D. S., Y. J. T., A. T., A. C. W., D. Wang, Y. W., M. W., S. K. W., M. Z.-W. and R. V. Data analysis: B. R., X.-C. H., J. S., L. D., L. C.-P., M. Simon, M. W. and S. K. W. Scientific discussion: B. R., X.-C. H., J. S., R. B., L. D., M. Sipilä., J. K., M. K., H. F., M. Simon, D. S., A. K., U. B., J. C., N. M. D., I. E. H., R. C. F., A. H., O. M., D. Worsnop and K. L. Writing: B. R., X.-C. H. and K. L.

Conflicts of interest

There are no conflicts of interest to declare.

Acknowledgements

We thank CERN for providing the facilities for the CLOUD experiments and the particle beam from the Proton Synchrotron. We are grateful to Andrea Baccarini (École polytechnique fédérale de Lausanne, Switzerland) and Julia Schmale (École

polytechnique fédérale de Lausanne, Switzerland) for providing the field data and the helpful discussions about nucleation in the Arctic. This work has received funding from the European Union's Horizon 2020 research and innovation program under the Marie Skłodowska-Curie grant agreement no 764991 (CLOUD-MOTION) and the Alfred Kordelin Foundation (grant no. 220257). We acknowledge the following projects: ACCC Flagship funded by the Research Council of Finland grant number 337549 (UH) and 337552 (FMI), Academy professorship funded by the Research Council of Finland (grant no. 302958), Research Council of Finland projects no. 1359331, 349659, 1325656, 311932, 334792, 316114, 325647, 325681, 347782, the Strategic Research Council (SRC) at the Academy of Finland (#352431), "Quantifying carbon sink, CarbonSink+ and their interaction with air quality" INAR project funded by Jane and Aatos Erkko Foundation, "Gigacity" project funded by Wihuri foundation, European Research Council (ERC) project ATM-GTP Contract no. 742206, European Union *via* Non-CO_2 Forcers and their Climate, Weather, Air Quality and Health Impacts (FOCI) and National Natural Science Foundation of China grant no. 42175118. Furthermore, this research has been funded by the Vienna Science and Technology Fund (WWTF) through project VRG22-003; the German Federal Ministry of Education and Research (BMBF) project nos. 01LK1601C, 01LK2201B, 01LK1601A and 01LK2201A, the Swiss National Science Foundation projects no. 200021_169090, 206021_198140, 200020_172602, 200021_213071 and 20FI20_172622, and the US National Science Foundation awards AGS-1801280, AGS-2215522, AGS-2027252, AGS-2215489, AGS-2132089, AGS-1602086, AGS-1801329 and AGS-2215527.

References

1 J. Haywood and O. Boucher, Estimates of the direct and indirect radiative forcing due to tropospheric aerosols: A review, *Rev. Geophys.*, 2000, **38**, 513–543.

2 J. Merikanto, D. V. Spracklen, G. W. Mann, S. J. Pickering and K. S. Carslaw, Impact of nucleation on global CCN, *Atmos. Chem. Phys.*, 2009, **9**, 8601–8616.

3 H. E. Manninen, T. Nieminen, E. Asmi, S. Gagné, S. Häkkinen, K. Lehtipalo, P. Aalto, M. Vana, A. Mirme, S. Mirme, U. Hõrrak, C. Plass-Dülmer, G. Stange, G. Kiss, A. Hoffer, N. Törő, M. Moerman, B. Henzing, G. de Leeuw, M. Brinkenberg, G. N. Kouvarakis, A. Bougiatioti, N. Mihalopoulos, C. O'Dowd, D. Ceburnis, A. Arneth, B. Svenningsson, E. Swietlicki, L. Tarozzi, S. Decesari, M. C. Facchini, W. Birmili, A. Sonntag, A. Wiedensohler, J. Boulon, K. Sellegri, P. Laj, M. Gysel, N. Bukowiecki, E. Weingartner, G. Wehrle, A. Laaksonen, A. Hamed, J. Joutsensaari, T. Petäjä, V.-M. Kerminen and M. Kulmala, EUCAARI ion spectrometer measurements at 12 European sites – analysis of new particle formation events, *Atmos. Chem. Phys.*, 2010, **10**, 7907–7927.

4 M. Dall'Osto, X. Querol, A. Alastuey, C. O'Dowd, R. M. Harrison, J. Wenger and F. J. Gómez-Moreno, On the spatial distribution and evolution of ultrafine particles in Barcelona, *Atmos. Chem. Phys.*, 2013, **13**, 741–759.

5 Z. Németh, B. Rosati, N. Zíková, I. Salma, L. Bozó, C. Dameto de España, J. Schwarz, V. Ždímal and A. Wonaschütz, Comparison of atmospheric new particle formation events in three Central European cities, *Atmos. Environ.*, 2018, **178**, 191–197.

6 Z. Wu, M. Hu, S. Liu, B. Wehner, S. Bauer, A. Ma ßling, A. Wiedensohler, T. Petäjä, M. Dal Maso and M. Kulmala, New particle formation in Beijing, China: Statistical analysis of a 1-year data set, *J. Geophys. Res.: Atmos.*, 2007, **112**(D9), DOI: 10.1029/2006JD007406.

7 D. L. Yue, M. Hu, R. Y. Zhang, Z. J. Wu, H. Su, Z. B. Wang, J. F. Peng, L. Y. He, X. F. Huang, Y. G. Gong and A. Wiedensohler, Potential contribution of new particle formation to cloud condensation nuclei in Beijing, *Atmos. Environ.*, 2011, **45**, 6070–6077.

8 S. Kecorius, T. Vogl, P. Paasonen, J. Lampilahti, D. Rothenberg, H. Wex, S. Zeppenfeld, M. van Pinxteren, M. Hartmann, S. Henning, X. Gong, A. Welti, M. Kulmala, F. Stratmann, H. Herrmann and A. Wiedensohler, New particle formation and its effect on cloud condensation nuclei abundance in the summer Arctic: a case study in the Fram Strait and Barents Sea, *Atmos. Chem. Phys.*, 2019, **19**, 14339–14364.

9 T. Jokinen, M. Sipilä, J. Kontkanen, V. Vakkari, P. Tisler, E.-M. Duplissy, H. Junninen, J. Kangasluoma, H. E. Manninen, T. Petäjä, M. Kulmala, D. R. Worsnop, J. Kirkby, A. Virkkula and V.-M. Kerminen, Ion-induced sulfuric acid–ammonia nucleation drives particle formation in coastal Antarctica, *Sci. Adv.*, 2018, **4**, eaat9744.

10 G. Zheng, Y. Wang, R. Wood, M. P. Jensen, C. Kuang, I. L. McCoy, A. Matthews, F. Mei, J. M. Tomlinson, J. E. Shilling, M. A. Zawadowicz, E. Crosbie, R. Moore, L. Ziemba, M. O. Andreae and J. Wang, New particle formation in the remote marine boundary layer, *Nat. Commun.*, 2021, **12**, 527.

11 M. D. Maso, L. Sogacheva, P. P. Aalto, I. Riipinen, M. Komppula, P. Tunved, L. Korhonen, V. Suur-Uski, A. Hirsikko, T. KurtéN, V.-M. Kerminen, H. Lihavainen, Y. Viisanen, H.-C. Hansson and M. Kulmala, Aerosol size distribution measurements at four Nordic field stations: identification, analysis and trajectory analysis of new particle formation bursts, *Tellus, Ser. B: Chem. Phys. Meteorol.*, 2007, **59**, 350–361.

12 J. Sulo, N. Sarnela, J. Kontkanen, L. Ahonen, P. Paasonen, T. Laurila, T. Jokinen, J. Kangasluoma, H. Junninen, M. Sipilä, T. Petäjä, M. Kulmala and K. Lehtipalo, Long-term measurement of sub-3 nm particles and their precursor gases in the boreal forest, *Atmos. Chem. Phys.*, 2021, **21**, 695–715.

13 M. Ehn, J. A. Thornton, E. Kleist, M. Sipilä, H. Junninen, I. Pullinen, M. Springer, F. Rubach, R. Tillmann, B. Lee, F. Lopez-Hilfiker, S. Andres, I.-H. Acir, M. Rissanen, T. Jokinen, S. Schobesberger, J. Kangasluoma, J. Kontkanen, T. Nieminen, T. Kurtén, L. B. Nielsen, S. Jørgensen, H. G. Kjaergaard, M. Canagaratna,

M. D. Maso, T. Berndt, T. Petäjä, A. Wahner, V.-M. Kerminen, M. Kulmala, D. R. Worsnop, J. Wildt and T. F. Mentel, A large source of low-volatility secondary organic aerosol, *Nature*, 2014, **506**, 476–479.

14 V.-M. Kerminen, T. Petäjä, H. E. Manninen, P. Paasonen, T. Nieminen, M. Sipilä, H. Junninen, M. Ehn, S. Gagné, L. Laakso, I. Riipinen, H. Vehkamäki, T. Kurten, I. K. Ortega, M. Dal Maso, D. Brus, A. Hyvärinen, H. Lihavainen, J. Leppä, K. E. J. Lehtinen, A. Mirme, S. Mirme, U. Hõrrak, T. Berndt, F. Stratmann, W. Birmili, A. Wiedensohler, A. Metzger, J. Dommen, U. Baltensperger, A. Kiendler-Scharr, T. F. Mentel, J. Wildt, P. M. Winkler, P. E. Wagner, A. Petzold, A. Minikin, C. Plass-Dülmer, U. Pöschl, A. Laaksonen and M. Kulmala, Atmospheric nucleation: highlights of the EUCAARI project and future directions, *Atmos. Chem. Phys.*, 2010, **10**, 10829–10848.

15 J. Kirkby, J. Curtius, J. Almeida, E. Dunne, J. Duplissy, S. Ehrhart, A. Franchin, S. Gagné, L. Ickes, A. Kürten, A. Kupc, A. Metzger, F. Riccobono, L. Rondo, S. Schobesberger, G. Tsagkogeorgas, D. Wimmer, A. Amorim, F. Bianchi, M. Breitenlechner, A. David, J. Dommen, A. Downard, M. Ehn, R. C. Flagan, S. Haider, A. Hansel, D. Hauser, W. Jud, H. Junninen, F. Kreissl, A. Kvashin, A. Laaksonen, K. Lehtipalo, J. Lima, E. R. Lovejoy, V. Makhmutov, S. Mathot, J. Mikkilä, P. Minginette, S. Mogo, T. Nieminen, A. Onnela, P. Pereira, T. Petäjä, R. Schnitzhofer, J. H. Seinfeld, M. Sipilä, Y. Stozhkov, F. Stratmann, A. Tomé, J. Vanhanen, Y. Viisanen, A. Vrtala, P. E. Wagner, H. Walther, E. Weingartner, H. Wex, P. M. Winkler, K. S. Carslaw, D. R. Worsnop, U. Baltensperger and M. Kulmala, Role of sulphuric acid, ammonia and galactic cosmic rays in atmospheric aerosol nucleation, *Nature*, 2011, **476**, 429–433.

16 X.-C. He, Y. J. Tham, L. Dada, M. Wang, H. Finkenzeller, D. Stolzenburg, S. Iyer, M. Simon, A. Kürten, J. Shen, B. Rörup, M. Rissanen, S. Schobesberger, R. Baalbaki, D. S. Wang, T. K. Koenig, T. Jokinen, N. Sarnela, L. J. Beck, J. Almeida, S. Amanatidis, A. Amorim, F. Ataei, A. Baccarini, B. Bertozzi, F. Bianchi, S. Brilke, L. Caudillo, D. Chen, R. Chiu, B. Chu, A. Dias, A. Ding, J. Dommen, J. Duplissy, I. El Haddad, L. Gonzalez Carracedo, M. Granzin, A. Hansel, M. Heinritzi, V. Hofbauer, H. Junninen, J. Kangasluoma, D. Kemppainen, C. Kim, W. Kong, J. E. Krechmer, A. Kvashin, T. Laitinen, H. Lamkaddam, C. P. Lee, K. Lehtipalo, M. Leiminger, Z. Li, V. Makhmutov, H. E. Manninen, G. Marie, R. Marten, S. Mathot, R. L. Mauldin, B. Mentler, O. Möhler, T. Müller, W. Nie, A. Onnela, T. Petäjä, J. Pfeifer, M. Philippov, A. Ranjithkumar, A. Saiz-Lopez, I. Salma, W. Scholz, S. Schuchmann, B. Schulze, G. Steiner, Y. Stozhkov, C. Tauber, A. Tomé, R. C. Thakur, O. Väisänen, M. Vazquez-Pufleau, A. C. Wagner, Y. Wang, S. K. Weber, P. M. Winkler, Y. Wu, M. Xiao, C. Yan, Q. Ye, A. Ylisirniö, M. Zauner-Wieczorek, Q. Zha, P. Zhou, R. C. Flagan, J. Curtius, U. Baltensperger, M. Kulmala, V.-M. Kerminen, T. Kurtén, N. M. Donahue, R. Volkamer, J. Kirkby, D. R. Worsnop and M. Sipilä, Role of iodine oxoacids in atmospheric aerosol nucleation, *Science*, 2021, **371**, 589–595.

17 T. Hoffmann, C. D. O'Dowd and J. H. Seinfeld, Iodine oxide homogeneous nucleation: An explanation for coastal new particle production, *Geophys. Res. Lett.*, 2001, **28**, 1949–1952.

18 C. D. O'Dowd, J. L. Jimenez, R. Bahreini, R. C. Flagan, J. H. Seinfeld, K. Hämeri, L. Pirjola, M. Kulmala, S. G. Jennings and T. Hoffmann, Marine aerosol formation from biogenic iodine emissions, *Nature*, 2002, **417**, 632–636.

19 M. Sipilä, N. Sarnela, T. Jokinen, H. Henschel, H. Junninen, J. Kontkanen, S. Richters, J. Kangasluoma, A. Franchin, O. Peräkylä, M. P. Rissanen, M. Ehn, H. Vehkamäki, T. Kurten, T. Berndt, T. Petäjä, D. Worsnop, D. Ceburnis, V.-M. Kerminen, M. Kulmala and C. O'Dowd, Molecular-scale evidence of aerosol particle formation *via* sequential addition of HIO3, *Nature*, 2016, **537**, 532–534.

20 H. Yu, L. Ren, X. Huang, M. Xie, J. He and H. Xiao, Iodine speciation and size distribution in ambient aerosols at a coastal new particle formation hotspot in China, *Atmos. Chem. Phys.*, 2019, **19**, 4025–4039.

21 X.-C. He, M. Simon, S. Iyer, H.-B. Xie, B. Rörup, J. Shen, H. Finkenzeller, D. Stolzenburg, R. Zhang, A. Baccarini, Y. J. Tham, M. Wang, S. Amanatidis, A. A. Piedehierro, A. Amorim, R. Baalbaki, Z. Brasseur, L. Caudillo, B. Chu, L. Dada, J. Duplissy, I. El Haddad, R. C. Flagan, M. Granzin, A. Hansel, M. Heinritzi, V. Hofbauer, T. Jokinen, D. Kemppainen, W. Kong, J. Krechmer, A. Kürten, H. Lamkaddam, B. Lopez, F. Ma, N. G. A. Mahfouz, V. Makhmutov, H. E. Manninen, G. Marie, R. Marten, D. Massabò, R. L. Mauldin, B. Mentler, A. Onnela, T. Petäjä, J. Pfeifer, M. Philippov, A. Ranjithkumar, M. P. Rissanen, S. Schobesberger, W. Scholz, B. Schulze, M. Surdu, R. C. Thakur, A. Tomé, A. C. Wagner, D. Wang, Y. Wang, S. K. Weber, A. Welti, P. M. Winkler, M. Zauner-Wieczorek, U. Baltensperger, J. Curtius, T. Kurtén, D. R. Worsnop, R. Volkamer, K. Lehtipalo, J. Kirkby, N. M. Donahue, M. Sipilä and M. Kulmala, Iodine oxoacids enhance nucleation of sulfuric acid particles in the atmosphere, *Science*, 2023, **382**, 1308–1314.

22 M. R. Grose, J. M. Cainey, A. McMinn and J. A. E. Gibson, Coastal marine methyl iodide source and links to new particle formation at Cape Grim during February 2006, *Environ. Chem.*, 2007, **4**, 172–177.

23 J. D. Allan, P. I. Williams, J. Najera, J. D. Whitehead, M. J. Flynn, J. W. Taylor, D. Liu, E. Darbyshire, L. J. Carpenter, R. Chance, S. J. Andrews, S. C. Hackenberg and G. McFiggans, Iodine observed in new particle formation events in the Arctic atmosphere during ACCACIA, *Atmos. Chem. Phys.*, 2015, **15**, 5599–5609.

24 A. Baccarini, L. Karlsson, J. Dommen, P. Duplessis, J. Vüllers, I. M. Brooks, A. Saiz-Lopez, M. Salter, M. Tjernström, U. Baltensperger, P. Zieger and J. Schmale, Frequent new particle formation over the high Arctic pack ice by enhanced iodine emissions, *Nat. Commun.*, 2020, **11**, 4924.

25 L. J. Beck, N. Sarnela, H. Junninen, C. J. M. Hoppe, O. Garmash, F. Bianchi, M. Riva, C. Rose, O. Peräkylä,

D. Wimmer, O. Kausiala, T. Jokinen, L. Ahonen, J. Mikkilä, J. Hakala, X.-C. He, J. Kontkanen, K. K. E. Wolf, D. Cappelletti, M. Mazzola, R. Traversi, C. Petroselli, A. P. Viola, V. Vitale, R. Lange, A. Massling, J. K. Nøjgaard, R. Krejci, L. Karlsson, P. Zieger, S. Jang, K. Lee, V. Vakkari, J. Lampilahti, R. C. Thakur, K. Leino, J. Kangasluoma, E.-M. Duplissy, E. Siivola, M. Marbouti, Y. J. Tham, A. Saiz-Lopez, T. Petäjä, M. Ehn, D. R. Worsnop, H. Skov, M. Kulmala, V.-M. Kerminen and M. Sipilä, Differing Mechanisms of New Particle Formation at Two Arctic Sites, *Geophys. Res. Lett.*, 2021, **48**, e2020GL091334.

26 L. J. Carpenter, S. M. MacDonald, M. D. Shaw, R. Kumar, R. W. Saunders, R. Parthipan, J. Wilson and J. M. C. Plane, Atmospheric iodine levels influenced by sea surface emissions of inorganic iodine, *Nat. Geosci.*, 2013, **6**, 108–111.

27 H. M. Atkinson, R.-J. Huang, R. Chance, H. K. Roscoe, C. Hughes, B. Davison, A. Schönhardt, A. S. Mahajan, A. Saiz-Lopez, T. Hoffmann and P. S. Liss, Iodine emissions from the sea ice of the Weddell Sea, *Atmos. Chem. Phys.*, 2012, **12**, 11229–11244.

28 J. C. Gómez Martín, T. R. Lewis, A. D. James, A. Saiz-Lopez and J. M. C. Plane, Insights into the Chemistry of Iodine New Particle Formation: The Role of Iodine Oxides and the Source of Iodic Acid, *J. Am. Chem. Soc.*, 2022, **144**, 9240–9253.

29 J. L. Jimenez, R. Bahreini, D. R. Cocker III, H. Zhuang, V. Varutbangkul, R. C. Flagan, J. H. Seinfeld, C. D. O'Dowd and T. Hoffmann, New particle formation from photooxidation of diiodomethane (CH_2I_2), *J. Geophys. Res.: Atmos.*, 2003, **108**(D10), DOI: 10.1029/2002JD002452.

30 R. W. Saunders and J. M. C. Plane, Formation Pathways and Composition of Iodine Oxide Ultra-Fine Particles, *Environ. Chem.*, 2005, **2**, 299–303.

31 J. B. Burkholder, J. Curtius, A. R. Ravishankara and E. R. Lovejoy, Laboratory studies of the homogeneous nucleation of iodine oxides, *Atmos. Chem. Phys.*, 2004, **4**, 19–34.

32 H. Finkenzeller, S. Iyer, X.-C. He, M. Simon, T. K. Koenig, C. F. Lee, R. Valiev, V. Hofbauer, A. Amorim, R. Baalbaki, A. Baccarini, L. Beck, D. M. Bell, L. Caudillo, D. Chen, R. Chiu, B. Chu, L. Dada, J. Duplissy, M. Heinritzi, D. Kemppainen, C. Kim, J. Krechmer, A. Kürten, A. Kvashnin, H. Lamkaddam, C. P. Lee, K. Lehtipalo, Z. Li, V. Makhmutov, H. E. Manninen, G. Marie, R. Marten, R. L. Mauldin, B. Mentler, T. Müller, T. Petäjä, M. Philippov, A. Ranjithkumar, B. Rörup, J. Shen, D. Stolzenburg, C. Tauber, Y. J. Tham, A. Tomé, M. Vazquez-Pufleau, A. C. Wagner, D. S. Wang, M. Wang, Y. Wang, S. K. Weber, W. Nie, Y. Wu, M. Xiao, Q. Ye, M. Zauner-Wieczorek, A. Hansel, U. Baltensperger, J. Brioude, J. Curtius, N. M. Donahue, I. E. Haddad, R. C. Flagan, M. Kulmala, J. Kirkby, M. Sipilä, D. R. Worsnop, T. Kurten, M. Rissanen and R. Volkamer, The gas-phase formation mechanism of iodic acid as an atmospheric aerosol source, *Nat. Chem.*, 2023, **15**, 129–135.

33 Y. Zhang, D. Li, X.-C. He, W. Nie, C. Deng, R. Cai, Y. Liu, Y. Guo, C. Liu, Y. Li, L. Chen, Y. Li, C. Hua, T. Liu, Z. Wang, L. Wang, T. Petäjä, F. Bianchi, X. Qi, X. Chi, P. Paasonen, Y. Liu, C. Yan, J. Jiang, A. Ding and M. Kulmala, *Iodine Oxoacids and Their Roles in Sub-3 Nanometer Particle Growth in Polluted Urban Environments*, EGUsphere, 2023, pp. 1–39.

34 L. Liu, S. Li, H. Zu and X. Zhang, Unexpectedly significant stabilizing mechanism of iodous acid on iodic acid nucleation under different atmospheric conditions, *Sci. Total Environ.*, 2023, **859**, 159832.

35 R. Zhang, H.-B. Xie, F. Ma, J. Chen, S. Iyer, M. Simon, M. Heinritzi, J. Shen, Y. J. Tham, T. Kurtén, D. R. Worsnop, J. Kirkby, J. Curtius, M. Sipilä, M. Kulmala and X.-C. He, Critical Role of Iodous Acid in Neutral Iodine Oxoacid Nucleation, *Environ. Sci. Technol.*, 2022, **56**, 14166–14177.

36 J. Almeida, S. Schobesberger, A. Kürten, I. K. Ortega, O. Kupiainen-Määttä, A. P. Praplan, A. Adamov, A. Amorim, F. Bianchi, M. Breitenlechner, A. David, J. Dommen, N. M. Donahue, A. Downard, E. Dunne, J. Duplissy, S. Ehrhart, R. C. Flagan, A. Franchin, R. Guida, J. Hakala, A. Hansel, M. Heinritzi, H. Henschel, T. Jokinen, H. Junninen, M. Kajos, J. Kangasluoma, H. Keskinen, A. Kupc, T. Kurtén, A. N. Kvashin, A. Laaksonen, K. Lehtipalo, M. Leiminger, J. Leppä, V. Loukonen, V. Makhmutov, S. Mathot, M. J. McGrath, T. Nieminen, T. Olenius, A. Onnela, T. Petäjä, F. Riccobono, I. Riipinen, M. Rissanen, L. Rondo, T. Ruuskanen, F. D. Santos, N. Sarnela, S. Schallhart, R. Schnitzhofer, J. H. Seinfeld, M. Simon, M. Sipilä, Y. Stozhkov, F. Stratmann, A. Tomé, J. Tröstl, G. Tsagkogeorgas, P. Vaattovaara, Y. Viisanen, A. Virtanen, A. Vrtala, P. E. Wagner, E. Weingartner, H. Wex, C. Williamson, D. Wimmer, P. Ye, T. Yli-Juuti, K. S. Carslaw, M. Kulmala, J. Curtius, U. Baltensperger, D. R. Worsnop, H. Vehkamäki and J. Kirkby, Molecular understanding of sulphuric acid–amine particle nucleation in the atmosphere, *Nature*, 2013, **502**, 359–363.

37 H. Zu, S. Zhang, L. Liu and X. Zhang, The vital role of sulfuric acid in iodine oxoacids nucleation: impacts of urban pollutants on marine atmosphere, *Environ. Res. Lett.*, 2024, **19**, 014076.

38 H. Zu, S. Zhang, S. Li, L. Liu and X. Zhang, The synergistic nucleation of iodous acid and sulfuric acid: A vital mechanism in polluted marine regions, *Atmos. Environ.*, 2024, **318**, 120266.

39 J. Kirkby, J. Duplissy, K. Sengupta, C. Frege, H. Gordon, C. Williamson, M. Heinritzi, M. Simon, C. Yan, J. Almeida, J. Tröstl, T. Nieminen, I. K. Ortega, R. Wagner, A. Adamov, A. Amorim, A.-K. Bernhammer, F. Bianchi, M. Breitenlechner, S. Brilke, X. Chen, J. Craven, A. Dias, S. Ehrhart, R. C. Flagan, A. Franchin, C. Fuchs, R. Guida, J. Hakala, C. R. Hoyle, T. Jokinen, H. Junninen, J. Kangasluoma, J. Kim, M. Krapf, A. Kürten, A. Laaksonen, K. Lehtipalo, V. Makhmutov, S. Mathot, U. Molteni, A. Onnela, O. Peräkylä, F. Piel, T. Petäjä, A. P. Praplan, K. Pringle, A. Rap, N. A. D. Richards, I. Riipinen, M. P. Rissanen, L. Rondo, N. Sarnela, S. Schobesberger, C. E. Scott, J. H. Seinfeld, M. Sipilä, G. Steiner, Y. Stozhkov, F. Stratmann, A. Tomé, A. Virtanen,

A. L. Vogel, A. C. Wagner, P. E. Wagner, E. Weingartner, D. Wimmer, P. M. Winkler, P. Ye, X. Zhang, A. Hansel, J. Dommen, N. M. Donahue, D. R. Worsnop, U. Baltensperger, M. Kulmala, K. S. Carslaw and J. Curtius, Ion-induced nucleation of pure biogenic particles, *Nature*, 2016, **533**, 521–526.

40 T. K. Koenig, S. Baidar, P. Campuzano-Jost, C. A. Cuevas, B. Dix, R. P. Fernandez, H. Guo, S. R. Hall, D. Kinnison, B. A. Nault, K. Ullmann, J. L. Jimenez, A. Saiz-Lopez and R. Volkamer, Quantitative detection of iodine in the stratosphere, *Proc. Natl. Acad. Sci. U. S. A.*, 2020, **117**, 1860–1866.

41 J. Duplissy, J. Merikanto, A. Franchin, G. Tsagkogeorgas, J. Kangasluoma, D. Wimmer, H. Vuollekoski, S. Schobesberger, K. Lehtipalo, R. C. Flagan, D. Brus, N. M. Donahue, H. Vehkamäki, J. Almeida, A. Amorim, P. Barmet, F. Bianchi, M. Breitenlechner, E. M. Dunne, R. Guida, H. Henschel, H. Junninen, J. Kirkby, A. Kürten, A. Kupc, A. Määttänen, V. Makhmutov, S. Mathot, T. Nieminen, A. Onnela, A. P. Praplan, F. Riccobono, L. Rondo, G. Steiner, A. Tome, H. Walther, U. Baltensperger, K. S. Carslaw, J. Dommen, A. Hansel, T. Petäjä, M. Sipilä, F. Stratmann, A. Vrtala, P. E. Wagner, D. R. Worsnop, J. Curtius and M. Kulmala, Effect of ions on sulfuric acid-water binary particle formation: 2. Experimental data and comparison with QC-normalized classical nucleation theory, *J. Geophys. Res.: Atmos.*, 2016, **121**, 1752–1775.

42 J. Vanhanen, J. Mikkilä, K. Lehtipalo, M. Sipilä, H. E. Manninen, E. Siivola, T. Petäjä and M. Kulmala, Particle Size Magnifier for Nano-CN Detection, *Aerosol Sci. Technol.*, 2011, **45**, 533–542.

43 J. Tröstl, T. Tritscher, O. F. Bischof, H.-G. Horn, T. Krinke, U. Baltensperger and M. Gysel, Fast and precise measurement in the sub-20nm size range using a Scanning Mobility Particle Sizer, *J. Aerosol Sci.*, 2015, **87**, 75–87.

44 S. Mirme and A. Mirme, The mathematical principles and design of the NAIS – a spectrometer for the measurement of cluster ion and nanometer aerosol size distributions, *Atmos. Meas. Tech.*, 2013, **6**, 1061–1071.

45 A. Kürten, T. Jokinen, M. Simon, M. Sipilä, N. Sarnela, H. Junninen, A. Adamov, J. Almeida, A. Amorim, F. Bianchi, M. Breitenlechner, J. Dommen, N. M. Donahue, J. Duplissy, S. Ehrhart, R. C. Flagan, A. Franchin, J. Hakala, A. Hansel, M. Heinritzi, M. Hutterli, J. Kangasluoma, J. Kirkby, A. Laaksonen, K. Lehtipalo, M. Leiminger, V. Makhmutov, S. Mathot, A. Onnela, T. Petäjä, A. P. Praplan, F. Riccobono, M. P. Rissanen, L. Rondo, S. Schobesberger, J. H. Seinfeld, G. Steiner, A. Tomé, J. Tröstl, P. M. Winkler, C. Williamson, D. Wimmer, P. Ye, U. Baltensperger, K. S. Carslaw, M. Kulmala, D. R. Worsnop and J. Curtius, Neutral molecular cluster formation of sulfuric acid–dimethylamine observed in real time under atmospheric conditions, *Proc. Natl. Acad. Sci. U. S. A.*, 2014, **111**, 15019–15024.

46 X.-C. He, J. Shen, S. Iyer, P. Juuti, J. Zhang, M. Koirala, M. M. Kytökari, D. R. Worsnop, M. Rissanen, M. Kulmala, N. M. Maier, J. Mikkilä, M. Sipilä and J. Kangasluoma, Characterisation of gaseous iodine species detection using the multi-scheme chemical ionisation inlet 2 with bromide and nitrate chemical ionisation methods, *Atmos. Meas. Tech.*, 2023, **16**, 4461–4487.

47 M. Wang, X.-C. He, H. Finkenzeller, S. Iyer, D. Chen, J. Shen, M. Simon, V. Hofbauer, J. Kirkby, J. Curtius, N. Maier, T. Kurtén, D. R. Worsnop, M. Kulmala, M. Rissanen, R. Volkamer, Y. J. Tham, N. M. Donahue and M. Sipilä, Measurement of iodine species and sulfuric acid using bromide chemical ionization mass spectrometers, *Atmos. Meas. Tech.*, 2021, **14**, 4187–4202.

48 L. Dada, K. Lehtipalo, J. Kontkanen, T. Nieminen, R. Baalbaki, L. Ahonen, J. Duplissy, C. Yan, B. Chu, T. Petäjä, K. Lehtinen, V.-M. Kerminen, M. Kulmala and J. Kangasluoma, Formation and growth of sub-3-nm aerosol particles in experimental chambers, *Nat. Protoc.*, 2020, **15**, 1013–1040.

49 M. Kulmala, T. Petäjä, T. Nieminen, M. Sipilä, H. E. Manninen, K. Lehtipalo, M. Dal Maso, P. P. Aalto, H. Junninen, P. Paasonen, I. Riipinen, K. E. J. Lehtinen, A. Laaksonen and V.-M. Kerminen, Measurement of the nucleation of atmospheric aerosol particles, *Nat. Protoc.*, 2012, **7**, 1651–1667.

50 R. Wagner, C. Yan, K. Lehtipalo, J. Duplissy, T. Nieminen, J. Kangasluoma, L. R. Ahonen, L. Dada, J. Kontkanen, H. E. Manninen, A. Dias, A. Amorim, P. S. Bauer, A. Bergen, A.-K. Bernhammer, F. Bianchi, S. Brilke, S. B. Mazon, X. Chen, D. C. Draper, L. Fischer, C. Frege, C. Fuchs, O. Garmash, H. Gordon, J. Hakala, L. Heikkinen, M. Heinritzi, V. Hofbauer, C. R. Hoyle, J. Kirkby, A. Kürten, A. N. Kvashnin, T. Laurila, M. J. Lawler, H. Mai, V. Makhmutov, R. L. Mauldin III, U. Molteni, L. Nichman, W. Nie, A. Ojdanic, A. Onnela, F. Piel, L. L. J. Quéléver, M. P. Rissanen, N. Sarnela, S. Schallhart, K. Sengupta, M. Simon, D. Stolzenburg, Y. Stozhkov, J. Tröstl, Y. Viisanen, A. L. Vogel, A. C. Wagner, M. Xiao, P. Ye, U. Baltensperger, J. Curtius, N. M. Donahue, R. C. Flagan, M. Gallagher, A. Hansel, J. N. Smith, A. Tomé, P. M. Winkler, D. Worsnop, M. Ehn, M. Sipilä, V.-M. Kerminen, T. Petäjä and M. Kulmala, The role of ions in new particle formation in the CLOUD chamber, *Atmos. Chem. Phys.*, 2017, **17**, 15181–15197.

51 K. Lehtipalo, M. Sipilä, I. Riipinen, T. Nieminen and M. Kulmala, Analysis of atmospheric neutral and charged molecular clusters in boreal forest using pulse-height CPC, *Atmos. Chem. Phys.*, 2009, **9**, 4177–4184.

52 X.-C. He, S. Iyer, M. Sipilä, A. Ylisirniö, M. Peltola, J. Kontkanen, R. Baalbaki, M. Simon, A. Kürten, Y. J. Tham, J. Pesonen, L. R. Ahonen, S. Amanatidis, A. Amorim, A. Baccarini, L. Beck, F. Bianchi, S. Brilke, D. Chen, R. Chiu, J. Curtius, L. Dada, A. Dias, J. Dommen, N. M. Donahue, J. Duplissy, I. El Haddad, H. Finkenzeller, L. Fischer, M. Heinritzi, V. Hofbauer, J. Kangasluoma, C. Kim, T. K. Koenig, J. Kubečka, A. Kvashnin, H. Lamkaddam, C. P. Lee, M. Leiminger, Z. Li, V. Makhmutov, M. Xiao, R. Marten, W. Nie, A. Onnela,

E. Partoll, T. Petäjä, V.-T. Salo, S. Schuchmann, G. Steiner, D. Stolzenburg, Y. Stozhkov, C. Tauber, A. Tomé, O. Väisänen, M. Vazquez-Pufleau, R. Volkamer, A. C. Wagner, M. Wang, Y. Wang, D. Wimmer, P. M. Winkler, D. R. Worsnop, Y. Wu, C. Yan, Q. Ye, K. Lehtinen, T. Nieminen, H. E. Manninen, M. Rissanen, S. Schobesberger, K. Lehtipalo, U. Baltensperger, A. Hansel, V.-M. Kerminen, R. C. Flagan, J. Kirkby, T. Kurtén and M. Kulmala, Determination of the collision rate coefficient between charged iodic acid clusters and iodic acid using the appearance time method, *Aerosol Sci. Technol.*, 2021, **55**, 231–242.

53 J. G. Crump and J. H. Seinfeld, Turbulent deposition and gravitational sedimentation of an aerosol in a vessel of arbitrary shape, *J. Aerosol Sci.*, 1981, **12**, 405–415.

54 H. Israël, *Atmosphärische Elektrizität*, Teil 1., Leitfähigkeit, Ionen, Akademische Verlagsgesellschaft Geest & Portig KG, 1957.

55 M. Zauner-Wieczorek, J. Curtius and A. Kürten, The ion–ion recombination coefficient α: comparison of temperature- and pressure-dependent parameterisations for the troposphere and stratosphere, *Atmos. Chem. Phys.*, 2022, **22**, 12443–12465.

56 R. A. Minzner, The 1976 Standard Atmosphere and its relationship to earlier standards, *Rev. Geophys.*, 1977, **15**, 375–384.

57 G. Kummerlöwe and M. K. Beyer, Rate estimates for collisions of ionic clusters with neutral reactant molecules, *Int. J. Mass Spectrom.*, 2005, **244**, 84–90.

58 A. Hirsikko, T. Nieminen, S. Gagné, K. Lehtipalo, H. E. Manninen, M. Ehn, U. Hõrrak, V.-M. Kerminen, L. Laakso, P. H. McMurry, A. Mirme, S. Mirme, T. Petäjä, H. Tammet, V. Vakkari, M. Vana and M. Kulmala, Atmospheric ions and nucleation: a review of observations, *Atmos. Chem. Phys.*, 2011, **11**, 767–798.

59 B. R'Mili, R. S. Strekowski, B. Temime-Roussel, H. Wortham and A. Monod, Important effects of relative humidity on the formation processes of iodine oxide particles from CH3I photo-oxidation, *J. Hazard. Mater.*, 2022, **433**, 128729.

60 H. Tammet, Size and mobility of nanometer particles, clusters and ions, *J. Aerosol Sci.*, 1995, **26**, 459–475.

61 L. Ahonen, C. Li, J. Kubečka, S. Iyer, H. Vehkamäki, T. Petäjä, M. Kulmala and C. J. Hogan Jr, Ion Mobility-Mass Spectrometry of Iodine Pentoxide–Iodic Acid Hybrid Cluster Anions in Dry and Humidified Atmospheres, *J. Phys. Chem. Lett.*, 2019, **10**, 1935–1941.

62 R. Zhang, A. Khalizov, L. Wang, M. Hu and W. Xu, Nucleation and Growth of Nanoparticles in the Atmosphere, *Chem. Rev.*, 2012, **112**, 1957–2011.

63 J. Elm, J. Kubečka, V. Besel, M. J. Jääskeläinen, R. Halonen, T. Kurtén and H. Vehkamäki, Modeling the formation and growth of atmospheric molecular clusters: A review, *J. Aerosol Sci.*, 2020, **149**, 105621.

64 S.-H. Lee, J. M. Reeves, J. C. Wilson, D. E. Hunton, A. A. Viggiano, T. M. Miller, J. O. Ballenthin and L. R. Lait, Particle Formation by Ion Nucleation in the Upper Troposphere and Lower Stratosphere, *Science*, 2003, **301**, 1886–1889.

65 N. G. A. Mahfouz and N. M. Donahue, Atmospheric Nanoparticle Survivability Reduction Due to Charge-Induced Coagulation Scavenging Enhancement, *Geophys. Res. Lett.*, 2021, **48**, e2021GL092758.

66 E. M. Dunne, H. Gordon, A. Kürten, J. Almeida, J. Duplissy, C. Williamson, I. K. Ortega, K. J. Pringle, A. Adamov, U. Baltensperger, P. Barmet, F. Benduhn, F. Bianchi, M. Breitenlechner, A. Clarke, J. Curtius, J. Dommen, N. M. Donahue, S. Ehrhart, R. C. Flagan, A. Franchin, R. Guida, J. Hakala, A. Hansel, M. Heinritzi, T. Jokinen, J. Kangasluoma, J. Kirkby, M. Kulmala, A. Kupc, M. J. Lawler, K. Lehtipalo, V. Makhmutov, G. Mann, S. Mathot, J. Merikanto, P. Miettinen, A. Nenes, A. Onnela, A. Rap, C. L. S. Reddington, F. Riccobono, N. A. D. Richards, M. P. Rissanen, L. Rondo, N. Sarnela, S. Schobesberger, K. Sengupta, M. Simon, M. Sipilä, J. N. Smith, Y. Stozkhov, A. Tomé, J. Tröstl, P. E. Wagner, D. Wimmer, P. M. Winkler, D. R. Worsnop and K. S. Carslaw, Global atmospheric particle formation from CERN CLOUD measurements, *Science*, 2016, **354**, 1119–1124.